JOURNAL OF GEOPHYSICAL RESEARCH, VOL. 112, D07108, doi:10.1029/2006JD007209, 2007

Scanning multichannel microwave radiometer snow water equivalent assimilation

Jiarui Dong,[1,2] Jeffrey P. Walker,[3] Paul R. Houser,[4] and Chaojiao Sun[2,5]

Received 16 February 2006; revised 7 December 2006; accepted 27 December 2006; published 10 April 2007.

[1] Accurate prediction of snowpack status is important for a range of environmental applications, yet model estimates are typically poor and in situ measurement coverage is inadequate. Moreover, remote sensing estimates are spatially and temporally limited due to complicating effects, including distance to open water, presence of wet snow, and presence of thick snow. However, through assimilation of remote sensing estimates into a land surface model, it is possible to capitalize on the strengths of both approaches. In order to achieve this, reliable estimates of the uncertainty in both remotely sensed and model simulated snow water equivalent (SWE) estimates are critical. For practical application, the remotely sensed SWE retrieval error is prescribed with a spatially constant but monthly varying value, with data omitted for (1) locations closer than 200 km to significant open water, (2) times and locations with model-predicted presence of liquid water in the snowpack, and (3) model SWE estimates greater than 100 mm. The model error is estimated using standard error propagation with a calibrated spatially and temporally constant model error contribution. A series of tests have been performed to assess the assimilation algorithm performance. Multiyear model simulations with and without remotely sensed SWE assimilation are presented and evaluated with in situ SWE observations. The SWE estimates from assimilation were found to be superior to both the model simulation and remotely sensed estimates alone, except when model SWE estimates rapidly and erroneously crossed the 100-mm SWE cutoff early in the snow season.

Citation: Dong, J., J. P. Walker, P. R. Houser, and C. Sun (2007), Scanning multichannel microwave radiometer snow water equivalent assimilation, *J. Geophys. Res.*, *112*, D07108, doi:10.1029/2006JD007209.

1. Introduction

[2] Previous modeling and observational studies have demonstrated that snow is an important climatic driver through the surface albedo's role in energy and water budgets [e.g., *Yeh et al.*, 1983; *Namias*, 1985; *Barnett et al.*, 1989; *Yang et al.*, 1999, 2001; *Cohen and Entekhabi*, 1999]. Models have an advantage over in situ observations in such climatic studies as they provide global estimates of the spatial and temporal variation in snowpack conditions, while in situ observations are limited in both space and time. Moreover, models are able to quantitatively describe the relationship between snowpack status and water and energy balance, enabling the climate system feedback to be fully explored. However, models are also limited by a number of factors. For example, successful snow evolution prediction is challenging due to immature knowledge of snow evolution physics, simplifications in model parameterizations, high spatial and temporal variability of snow cover, and errors in the model forcing data [e.g., *Lynch-Stieglitz*, 1994; *Rodell et al.*, 2004].

[3] Space-borne passive microwave sensors provide an alternate capability to monitor global-scale snow evolution, yielding 1- to 3-day repeat snow water equivalent (SWE) measurements at approximately 25- to 50-km resolution. Such sensors include the scanning multichannel microwave radiometer (SMMR), the special sensor microwave imager (SSM/I), and the advanced microwave scanning radiometer for the Earth (AMSR-E) observing system. Many investigators have carefully evaluated the accuracy of remotely sensed SWE, suggesting good prairie region performance but poor boreal forest and high latitude tundra region performance [e.g., *Robinson et al.*, 1993; *Tait and Armstrong*, 1996]. To overcome these limitations, *Foster et al.* [2005] derived an alternate algorithm that made systematic error adjustments based on environmental factors including forest cover and snow morphology (i.e., crystal size as a function of location and time of year). While this yielded an improvement in SWE estimates, the SWE estimates were affected by signal saturation above a SWE of approximately 100 mm,

[1]Hydrological Sciences Branch, NASA Goddard Space Flight Center, Greenbelt, Maryland, USA.
[2]Goddard Earth Sciences and Technology Center, University of Maryland Baltimore Country, Baltimore, Maryland, USA.
[3]Department of Civil and Environmental Engineering, The University of Melbourne, Parkville, Victoria, Australia.
[4]Climate Dynamics Department, College of Science, George Mason University and Center for Research on Environment and Water, Calverton, Maryland, USA.
[5]Global Modeling and Assimilation Office, NASA Goddard Space Flight Center, Greenbelt, Maryland, USA.

0148-0227/07/2006JD007209$09.00

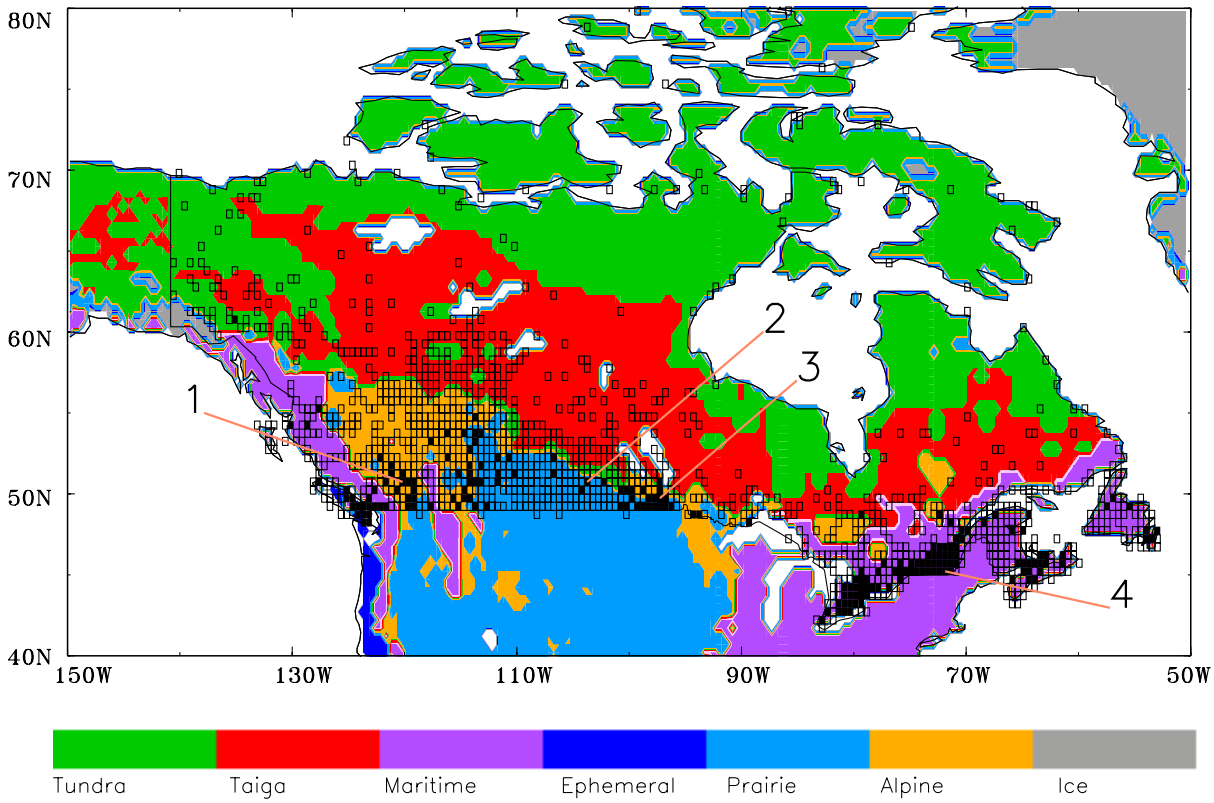

Figure 1. Spatial distribution of all half-degree by half-degree grid cells including one to four in situ SWE stations (open squares) and five or more in situ stations (solid squares), with the background colors showing snow classification according to *Sturm et al.* [1995]. The numbers 1 to 4 indicate selected pixels used in subsequent analysis.

mixed pixel contamination for regions within 200 km of large, open water bodies, and liquid water in the snowpack for monthly air temperatures above −2°C [*Dong et al.*, 2005]. Although this limits the use of remotely sensed SWE estimates to inland locations for times of moderate snowpack amount, it is at these times and locations that the snowpack is typically the most dynamic and model estimates are the poorest [e.g., *Slater et al.*, 2001].

[4] As both model predictions and remotely sensed estimates are characterized by different uncertainties at different times and locations, the most accurate snowpack status estimate results from the assimilation of remotely sensed estimates into a land surface model, with correct observation and model error specifications. The SWE estimation improvement using data assimilation can be verified using nonassimilated in situ data. In order to attain this optimal snowpack state estimate, it is essential that the assimilation scheme account for the relative uncertainty of both model predictions and observations. For example, direct replacement of the modeled snow states with observations by assuming that the observations are without any error can often yield degraded model predictions in certain situations [e.g., *Liston et al.*, 1999; *Rodell and Houser*, 2004]. Moreover, direct replacement of SWE has only a minimal impact on errors of correlated snow state estimates, such as snowpack depth and temperature.

[5] Several recent studies have applied the Kalman filter to the assimilation of snow cover and snow water equivalent in land surface and hydrological models, and their synthetic experiments showed improved streamflow and SWE simulation accuracy [*Sun et al.*, 2004; *Andreadis and Lettenmaier*, 2006; *Clark et al.*, 2006; *Slater and Clark*, 2006]. An advanced assimilation system has recently been developed to perform SWE assimilation with a one-dimensional extended Kalman filter (EKF) by *Sun et al.* [2004]. Their results from a series of identical-twin experiments have clearly demonstrated that poor initial condition effects can be removed, and runoff and atmospheric flux predictions improved in the absence of significant model and/or observation error [*Sun et al.*, 2004]. As significant model and remotely sensed SWE errors often exist in reality, assimilation of satellite-derived SWE and verification with actual in situ observations are challenging.

[6] Quantifying the observation and model uncertainties in a meaningful way is an important prerequisite to undertaking assimilation. While *Dong et al.* [2005] have made a thorough uncertainty assessment of *Foster et al.*'s [2005] semiempirical SWE retrieval algorithm which was used in this study, some of their recommendations for uncertainty assessment have required refinement for routine data assimilation application. Moreover, the model error parameter in the assimilation system designed by *Sun et al.* [2004] has been calibrated against observations

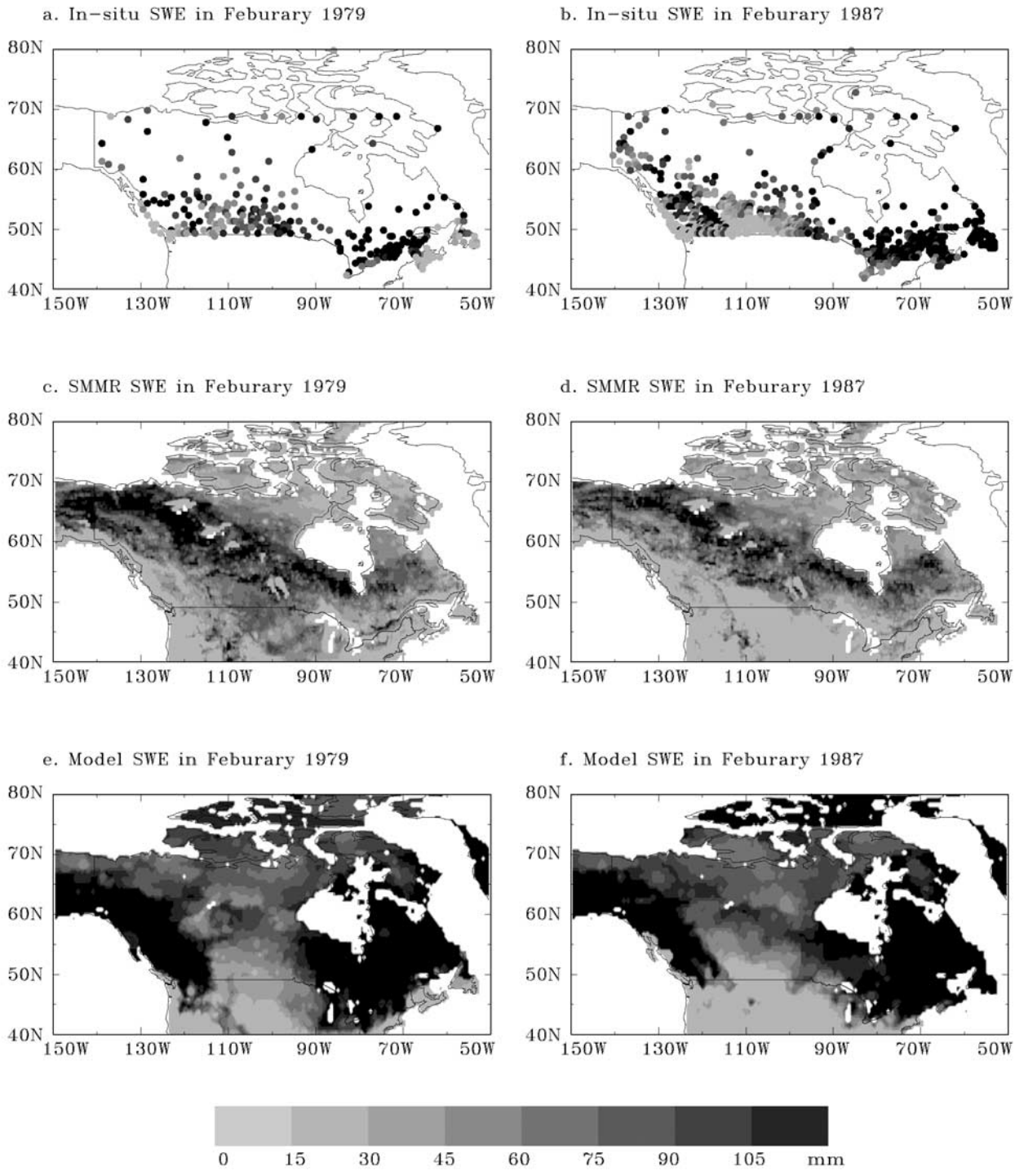

Figure 2. Map showing average values for February: (a) in situ SWE averaged to half-degree grid cells in 1979 and (b) 1987; (c) SMMR passive microwave SWE estimates in 1979 and (d) 1987; and (e) model simulated SWE in 1979 and (f) 1987.

to ensure realistic SWE error forecasts. The purpose of this paper is to demonstrate the expected SWE prediction improvement when remotely sensed SWE data are assimilated into a land surface model. This is the first study to assimilate SMMR-derived SWE estimates and to evaluate results against in situ SWE observations. Moreover, this North American demonstration study illustrates the water and energy budget impacts that can be

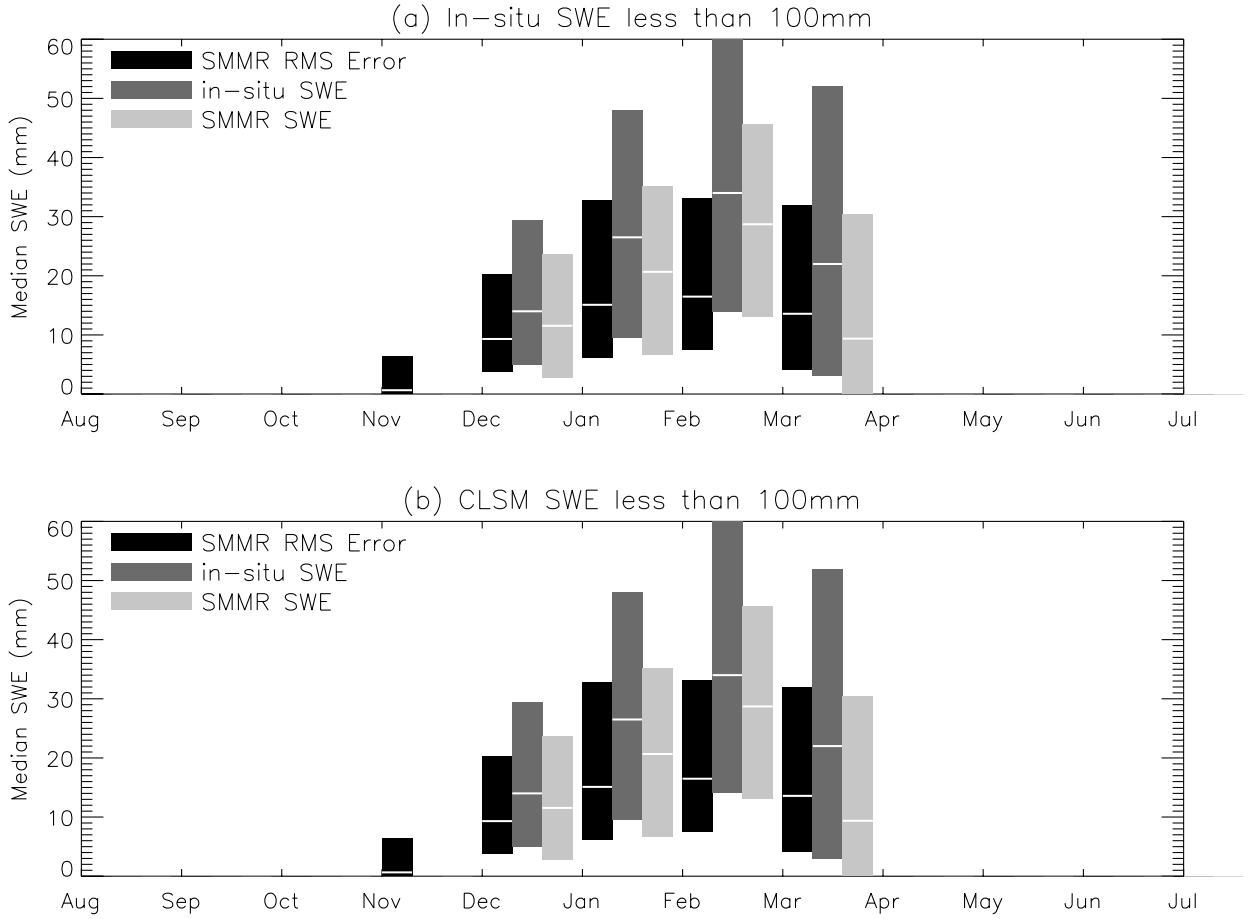

Figure 3. Comparison of monthly climatological median SMMR root mean square retrieval error, in situ SWE, and SMMR SWE estimates for pixels including five or more ground stations and farther than 200 km from open water, with an average monthly daytime temperature below −2°C, and (a) an in situ SWE estimate of less than 100 mm or (b) a model SWE prediction less than 100 mm. The white lines are the median values while the shaded regions show the range between upper and lower quartiles.

expected from the assimilation of remotely sensed SWE estimates.

2. Data and Model

2.1. In Situ Snow Observations

[7] This paper uses the Canadian Snow Water Equivalent Database estimates [*Brown*, 1996] for remotely sensed and model SWE uncertainty characterization and assimilation evaluation. This data set was chosen because of the spatially dense monitoring network and better overlap with the SMMR period than other available snow data sets. These SWE data were derived from the Meteorological Service of Canada (MSC) daily snow depth observation network, using an interpolated snow density from the snow survey network that was specifically designed to represent local terrain and vegetation. The resulting SWE estimates are reported to effectively represent observed spatial and temporal snow depth variability [*Brown and Braaten*, 1998; *Brown*, 2000; *Mote et al.*, 2003]. These Canadian snow observations are spatially dense in the southern more populated regions and sparse further to the north (Figure 1).

[8] While there is a recognized spatial discrepancy between the in situ observing station point measurements, the spatially averaged remote sensing retrieval, and model SWE simulation, this is the best verification data available. *Chang et al.* [2005] suggested that 10 distributed snow depth measurements per one-degree by one-degree grid cell are required to produce a sampling error of 5 cm or better. To minimize this discrepancy, in situ station SWE measurements within half-degree by half-degree (approximately 50 km by 35 km at 50°N) pixels were averaged, resulting in 1359 pixel averages having one or more stations. Figure 1 shows the pixels that include five or more in situ stations, with background colors showing snow classification as defined by *Sturm et al.* [1995]. There is a total 190 pixels that include five or more stations, with most pixels located in Prairie (28 pixels), Alpine (39 pixels), and Maritime (94 pixels) snow classes. Of these, four pixels have been selected for detailed analysis, one in Prairie, two in Alpine, and one in Maritime. Figures 2a and 2b show an example of in situ SWE data averaged to half-degree grid cells for February 1979 and 1987, respectively.

2.2. Passive Microwave Observations

[9] Several SWE estimation algorithms have been developed for passive microwave observations. The commonly used algorithm developed by *Chang et al.* [1987] estimates

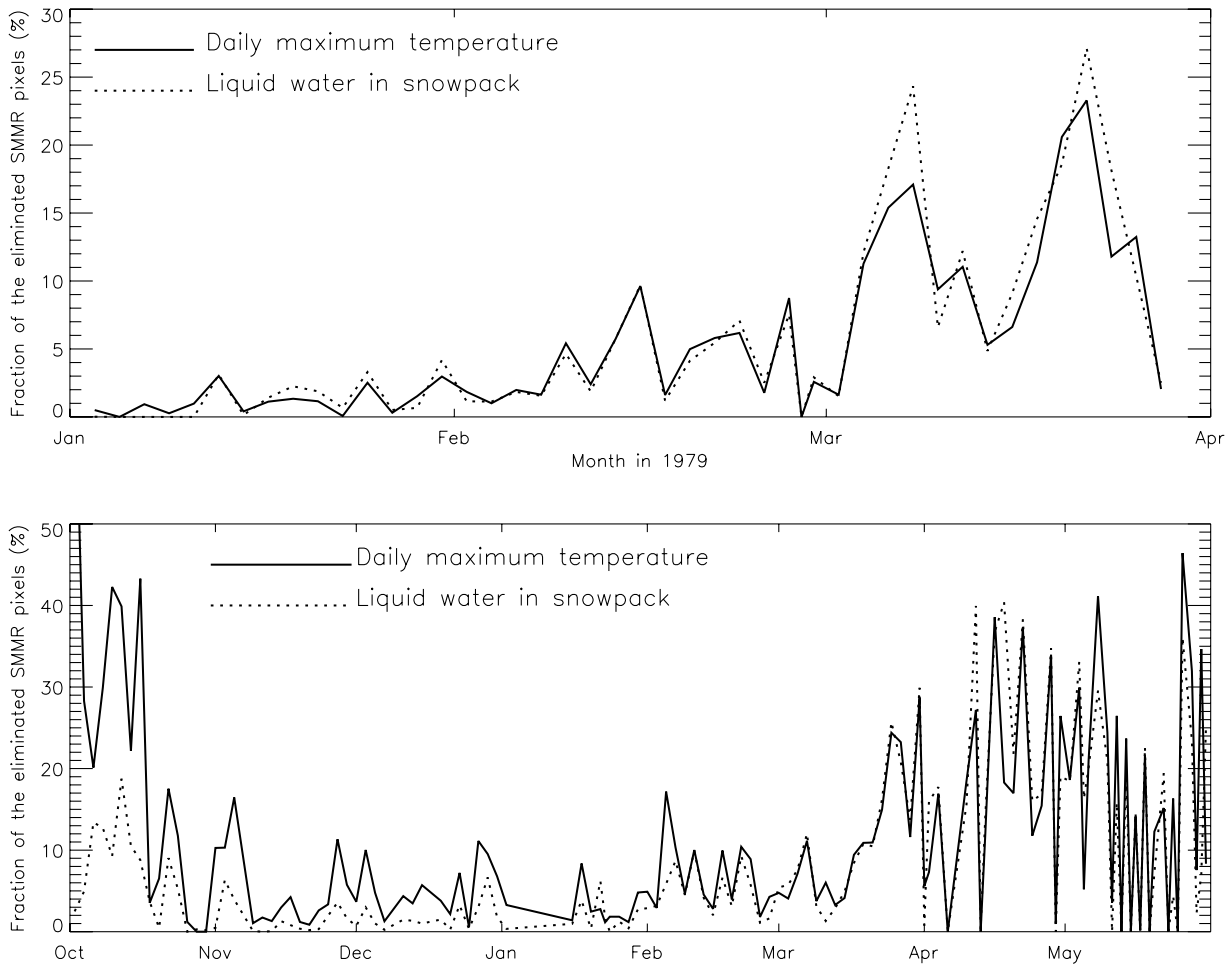

Figure 4. Comparison of fraction of snow-covered SMMR pixels eliminated by using either daily maximum temperature greater than −2°C as an indicator of liquid water in the snowpack or a land surface model liquid water diagnostic for (upper panel) January to March 1979 and (lower panel) October 1986 to May 1987.

SWE from the SMMR 18 and 37-GHz or SSM/I 19 and 37-GHz brightness temperature difference, multiplied by a constant derived from radiative transfer theory; the 37-GHz data are sensitive to snowpack scattering, while the 18-GHz data are relatively unaffected. In this paper, we use the algorithm developed by *Foster et al.* [2005] who modified the algorithm of *Chang et al.* [1987] using spatially and temporally varying constants to account for the effect of forest cover and snow crystal size.

$$\mathrm{SWE} = F\,c(T_{18} - T_{37}), \tag{1}$$

where F is the fractional forest cover factor calculated using the International Geosphere–Biosphere Program (IGBP) land cover map described by *Loveland et al.* [2000], and c is parameterized according to the Sturm snow class categories [*Sturm et al.*, 1995] and time of year. T_{18} and T_{37} are the horizontally polarized brightness temperatures at 18 and 37 GHz, respectively. Daytime SMMR observations and T_{37} observations greater than 240 K were excluded to partly minimize wet snow effects resulting from meltwater in the snowpack. Figures 2c and 2d show an example of SMMR SWE estimates by *Foster et al.* [2005] averaged over February in 1979 and 1987, respectively. The SMMR-derived SWE shows a close agreement with in situ data in the prairie and taiga regions but shows a significant underestimation in the east coast maritime region.

2.3. Snow Model and Assimilation Scheme

[10] The three-layer snow model of *Lynch-Stieglitz* [1994] used by the catchment-based land surface model of *Koster et al.* [2000] accounts for snowmelting and refreezing, dynamic changes in snow density, snow insulating properties, and other physics relevant to the growth and ablation of the snowpack. A novel component of this model is the nontraditional shape of the land surface element, defined to be the hydrological catchment. In this application, about 5000 catchments are used to model the North American continent, with an average catchment size of 3600 km^2. An internal mapping routine allows quantities on the irregular catchment domain to be communicated to and from a regular grid. This mapping routine uses an area-weighted average to undertake the mapping. The forcing data used in this study are from the 1.125 degrees 1979–1993 observationally corrected European Centre for Medium-Range Weather Forecasts (ECMWF) 15-year Re-analysis

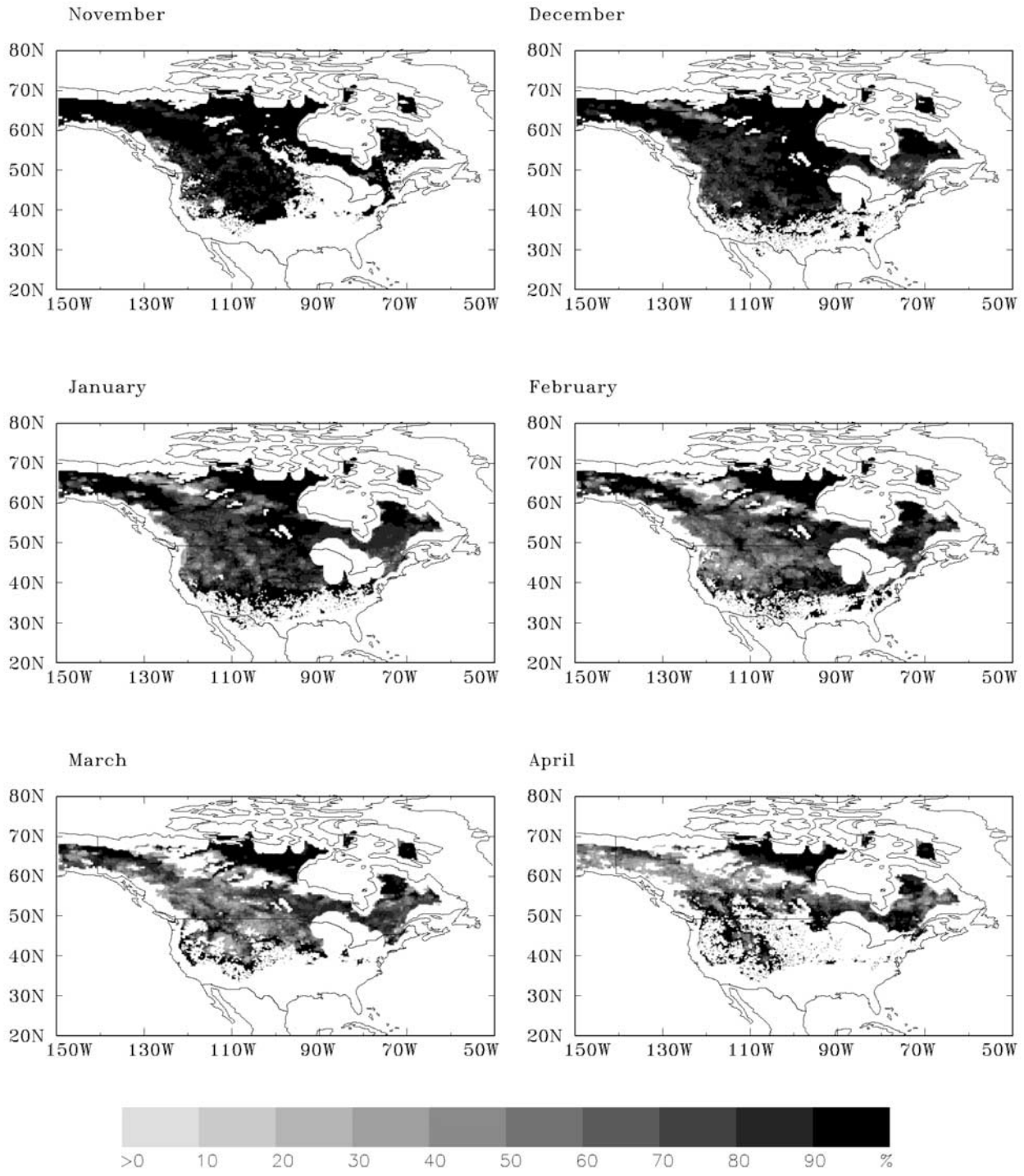

Figure 5. Monthly climatological maps showing the fraction of SMMR SWE retrievals that can ultimately be used for assimilation after accounting for distance to open water, signal saturation due to SWE amount, and liquid water presence.

(ERA-15) data set [*Berg et al.*, 2003]. Figure 2 compares model SWE estimates with in situ data and SMMR retrievals averaged over February in 1979 and 1987, respectively. These spatial representations of model SWE are quite "smooth" when compared to the remotely sensed estimates. While the SWE predicted by the model in Figure 2 agrees closely with in situ data for the southeast maritime regions, it is significantly overestimated in the west coast regions.

[11] Here we use the assimilation system recently developed by *Sun et al.* [2004] to assimilate SMMR-derived SWE observations. This assimilation scheme uses a one-dimensional extended Kalman filter to sequentially update the model state and covariance estimates as remotely sensed

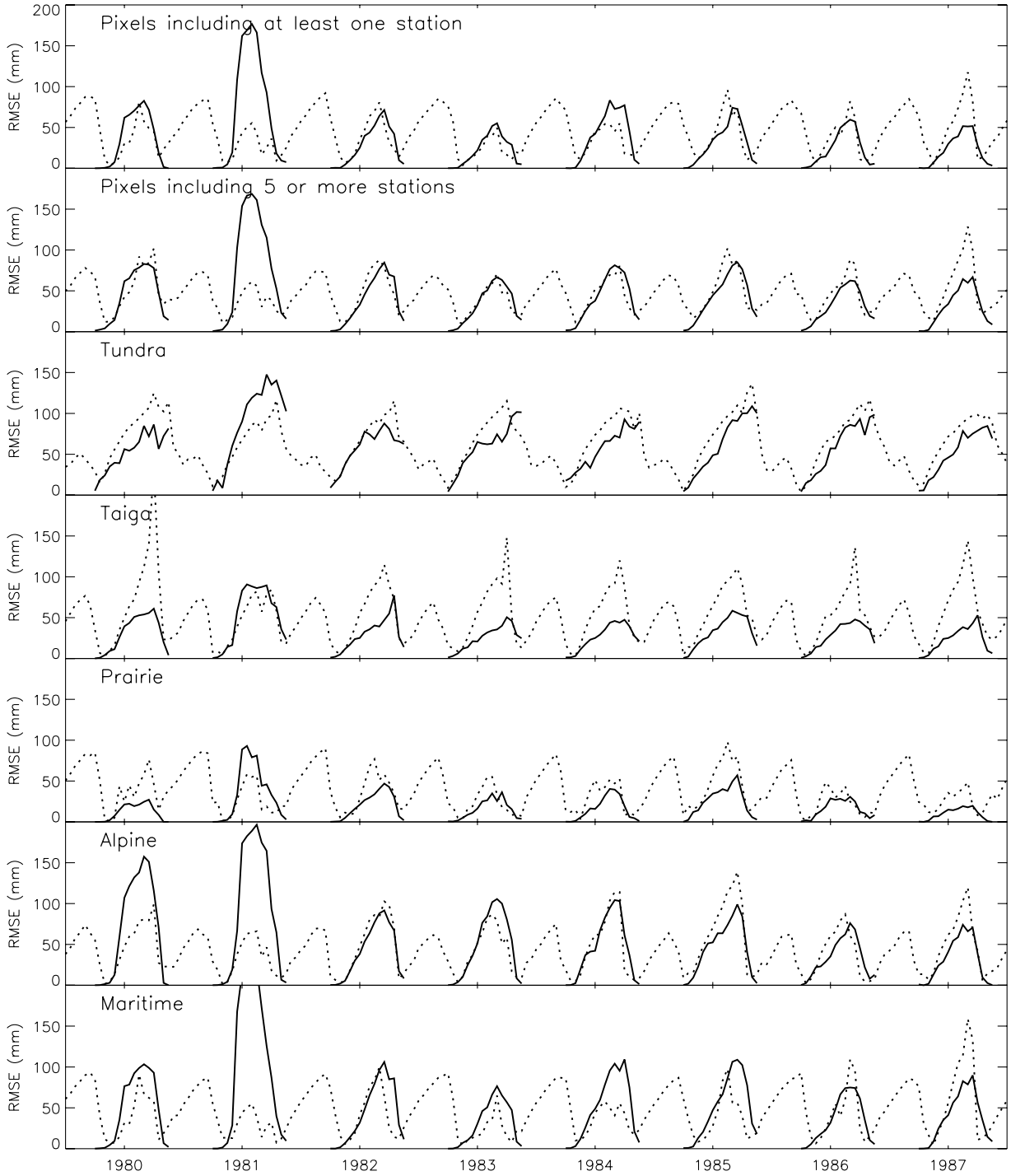

Figure 6. Comparison of predicted (dash lines) and actual model error estimates (solid lines; defined as root mean square error (RMSE) between the simulated SWE and the ground SWE observations) averaged for all the pixels including at least one station (top row), five or more stations (second row) and for each Sturm snow class (other rows).

SWE estimates become available. The EKF is a linearized statistical approach that provides a near-optimal state estimate of a nonlinear system, based on the relative magnitudes of the covariance of both the model system state estimate and the observations [e.g., *Gelb*, 1974]. Recent applications show that the principal advantage of this approach is that the EKF provides a framework within which the entire system is modified, with covariances representing the reliability of the observations and model predictions [*Houser et al.*, 1998; *Walker and Houser*, 2001; *Sun et al.*, 2004].

[12] Snow water equivalent together with heat content and snow depth describes the snowpack in the scheme designed by *Lynch-Stieglitz* [1994]. *Sun et al.* [2004]

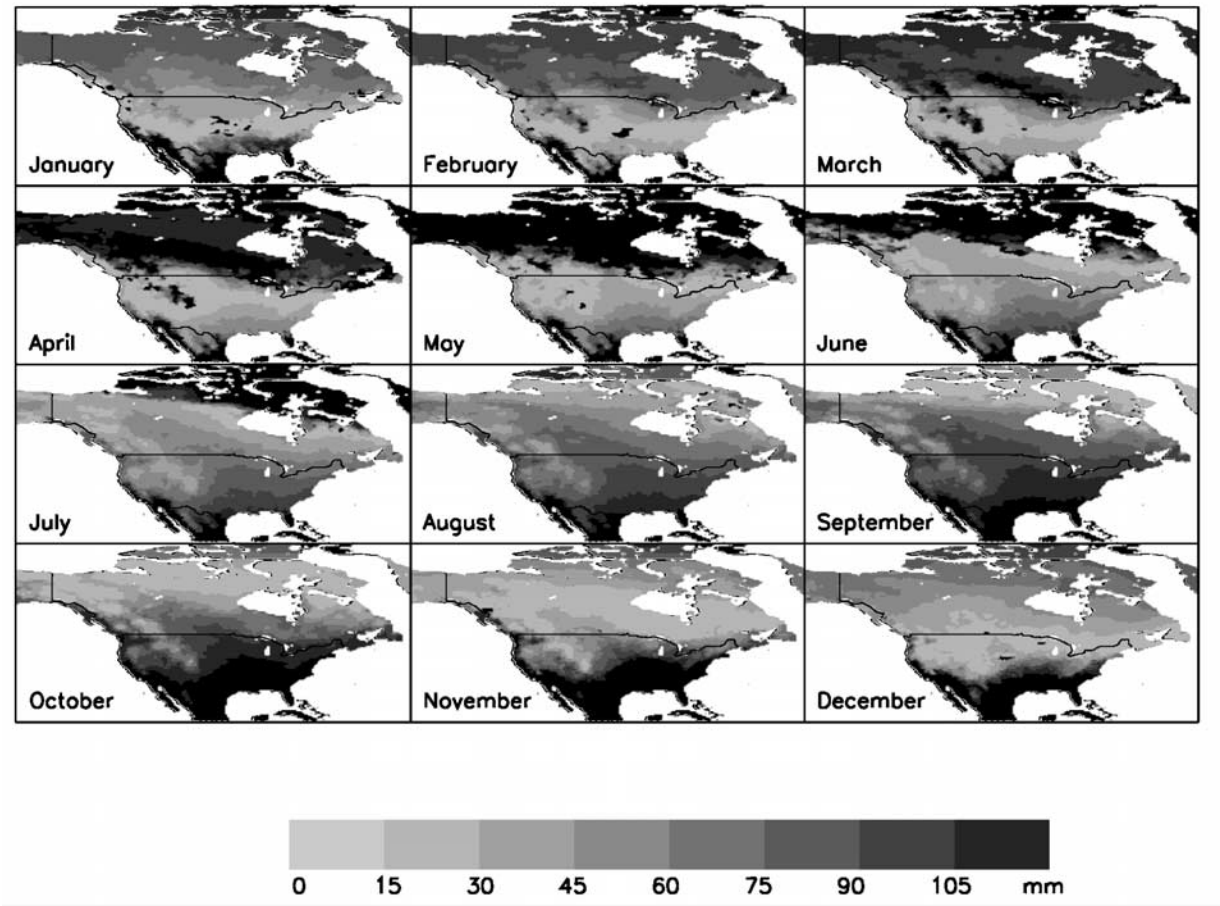

Figure 7. Monthly climatological maps of extended Kalman filter model error estimates.

designed a scheme that assimilates and updates the total catchment SWE, then updates snow depth and heat content in each layer by using the model-predicted snow temperature and density. This innovative approach is suitable for assimilating SMMR observations (since SMMR measures the total snowpack SWE) and overcomes the difficulty associated with model layer geometry and unique snow processes related to ablation. A full land surface model, snow model, and data assimilation system description are given in the papers noted above, so only the pertinent details are given here. Moreover, a detailed summary of the snow model is also given in the study by *Sun et al.* [2004].

3. Error Assessment

3.1. Remotely Sensed SWE Error Estimates

[13] Based on an extensive evaluation of SMMR SWE estimates using the algorithm by *Foster et al.* [2005] with in situ observations, *Dong et al.* [2005] suggest that SMMR SWE retrievals should not be used for (1) regions within 200 km of significant open water bodies due to mixed pixel contamination, (2) times when monthly mean air temperature is above -2°C due to potential meltwater contamination, and (3) times and locations where in situ SWE values are above 100 mm due to microwave signal saturation. Restricting the use of remotely sensed SWE on this basis was found to result in a nearly unbiased SWE estimate with seasonal maximum 20 mm RMS median error (Figure 3a). The monthly root mean square error (RMSE) median of SMMR SWE retrievals was obtained by first calculating the RMSE in each pixel over the entire SMMR period (1979–1987) and then obtaining the median among the pixels including five or more in situ stations.

[14] While imposing these rules on the remotely sensed SWE product makes it useful for practical applications, global application is difficult. For example, the 100-mm SWE cutoff rule requires prior knowledge of the actual SWE amount, which is only available at in situ measurement stations. Therefore a surrogate, such as the remotely sensed or model SWE, is required to replace the in situ SWE data. The problem with using the remotely sensed SWE is that deep snowpacks were significantly underestimated. However, use of model SWE in place of the in situ SWE (even without assimilation) was found to have a similar effect on eliminating erroneous remotely sensed SWE estimates in deep snowpack regions (Figure 3b).

[15] The other rule to be revised was the temperature cutoff, as snowmeltwater and refreezing ice both degrade the resultant SWE estimate. The presence of meltwater in the snowpack raises the 37-GHz microwave brightness temperature, and the refreezing ice crust results in the microwave signals having similar responses at the two frequencies [*Foster et al.*, 2005]. While climatological air temperature is a good indicator of the presence of meltwater, it does not contain information on the melt history and likely presence of ice. In contrast, the snow model keeps

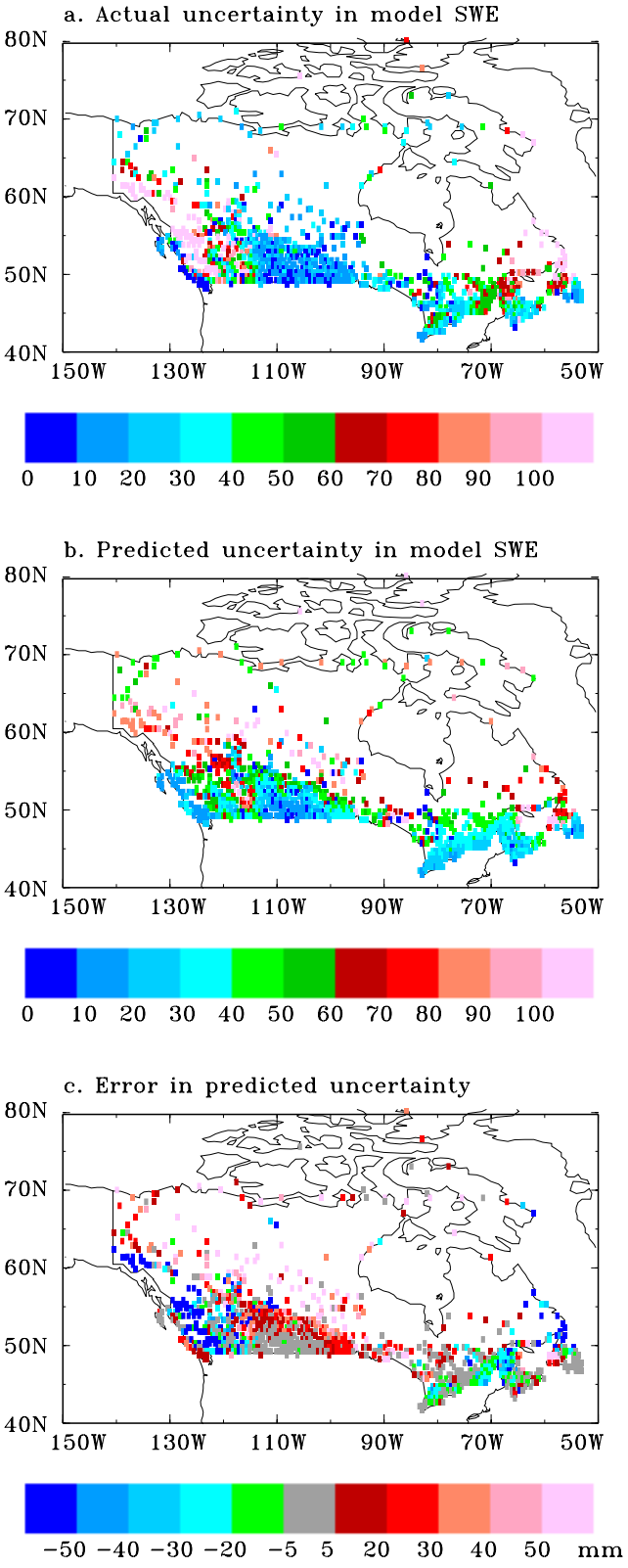

Figure 8. Climatological maps of (a) observed and (b) predicted model uncertainty for half-degree pixels with coincident ground truth observations for the winter season (November to April) during the period of 1979 to 1987; (c) error in predicted uncertainty.

track of snowpack liquid water content through consideration of meltwater generation, refreezing, and losses from evaporation and runoff when the liquid water exceeds the snowpack holding capacity. Therefore using the model simulated snowpack liquid water should be a better descriptor for eliminating contaminated remotely sensed retrievals due to wet snow effects than using air temperature data.

[16] The difference in the number of eliminated SMMR pixels between the two approaches is minor, with the exception of autumn and spring months (Figure 4). The large difference in these months is typically due to the absence of modeled snow (thus no liquid water in snowpack) in such pixels and air temperature greater than −2°C. Therefore the air temperature diagnostic is used as the default to determine observation quality when there is no model snow presence in the pixel. The differences found during midwinter months indicate that the air temperature diagnostic is typically conservative, meaning that some good data are eliminated. The exception is March 1979, where the temperature diagnostic missed some melt events. Therefore overall the use of modeled meltwater is an enhancement over the use of air temperature data for quality control on remotely sensed SWE.

[17] The average monthly varying RMS errors in the SMMR SWE estimates shown in Figure 3b are used to represent the passive microwave SMMR SWE estimate uncertainties in the regions beyond 200 km of significant open water bodies, locations and times with no liquid water presence in the snowpack, and the model SWE values below 100 mm. Figure 5 shows the average fraction of SMMR SWE retrievals used in the assimilation for each winter month based on the above three rules. Beyond the coastal areas, reliable SMMR SWE retrievals were available at most regions in November, December, January, and February, with reduced areas in March and April. The reduced percentage of SMMR SWE data available for use in assimilation during January and February when compared to November and December is due to the model SWE 100-mm cutoff. The reduced areas in March and April are due to the effects of liquid water presence in the snowpack. As will be demonstrated later, the reliable SMMR SWE data during the early snow season (November and December) play the most important role in the assimilation.

3.2. Modeled SWE Error Estimates

[18] Model-predicted total SWE (P^f) uncertainty estimates are propagated forward in time from the land surface dynamics using the EKF forecast equations (equation (4) in the study of *Sun et al.* [2004]). However, accurate estimation of the model error covariance (Q) is the most difficult task of any data assimilation problem, since it requires knowledge of the "truth" model states, which are typically unknown. Model forecast error may result from various sources, such as forcing data, model physics, and model parameters. While each of these components could be treated explicitly, the approach taken is to use a lumped predefined constant error term. Here applicability of the $(10\ \text{mm})^2$ value per 20 min chosen by *Sun et al.* [2004] in their identical-twin experiments is investigated for assimilating SMMR data, subject to an initial error estimate of $(20\ \text{mm})^2$. This is tested using the EKF forecast equations without assimilating any data.

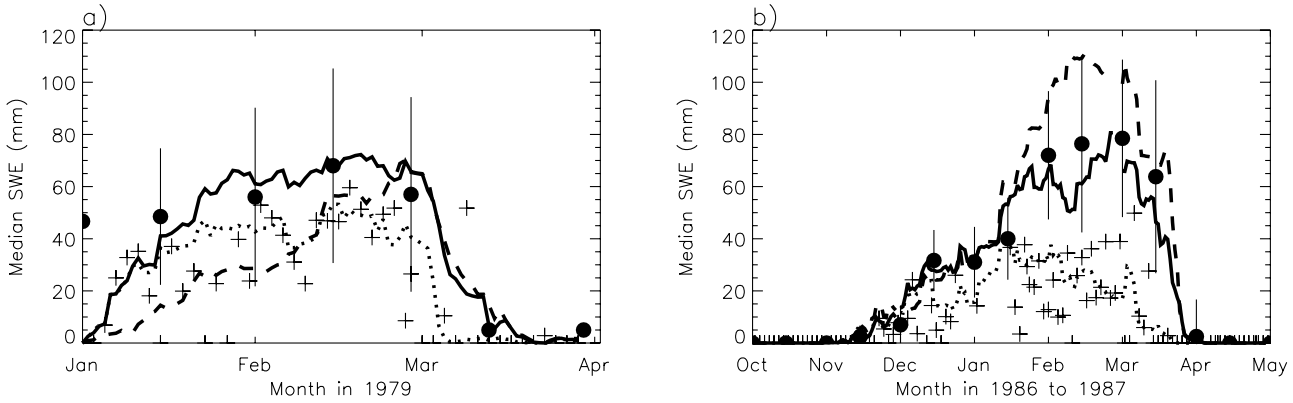

Figure 9. Comparison of the median SWE for pixels including five or more stations; ground observations (black dots), SMMR observations (plus), model forecast (dash lines), model forecast with assimilation run-I (dotted lines) and run-II (solid lines) from (a) January to March in 1979 and (b) from July 1986 to June 1987 (zoomed to the winter months from October 1986 to April 1987). The vertical lines show plus and minus one standard deviation from the median of ground observations.

[19] Comparison of predicted uncertainty with observed uncertainty [defined as root mean square error (RMSE) between the model and in situ SWE] found that the model forecast error globally overestimated the observed uncertainty by about 10 times (not shown) when using the default values. However, the predicted uncertainty temporal evolution agreed well with the observed uncertainty at seasonal scales. Therefore the globally constant error covariance was reduced to $(1\ \text{mm})^2$ from the value of $(10\ \text{mm})^2$ per 20 min. Using the revised error values, a close agreement was found between the predicted and observed model uncertainty (Figure 6). Moreover, a good agreement was found for the different snow class categories with the exception of Taiga, where model-predicted uncertainty remained larger than observed uncertainty. The summertime model-predicted uncertainty increase is an artifact of the error propagation as discussed below and the fact that there is no assimilation during that period. Consequently, there is always a large model-predicted uncertainty for the start of each snow season.

[20] Figure 7 shows monthly model forecast error spatial distributions averaged over the 1979–1987 period, with obvious spatial and temporal variations. Since the Kalman filter is designed to propagate the uncertainty, the model error is steadily increased according to the model error variance (during snow free periods) and model physics (during snow periods). In November, there are very small errors predicted in model estimates for almost all regions in Canada and the mountainous areas in the United States due to the earlier model snow presence. However, these areas are also among those with the largest errors in April due to the deeper snowpacks there in late winter. The largest forecast model uncertainty exists during summer no-snow periods and winter deep-snow periods. While the large summertime uncertainty may be unrealistic, a result of using a constant model error term, it is not considered to be a bad approximation for this demonstration study. One reason for this assertion is that the model error covariance is typically initialized high in data assimilation studies such as this, to represent the large degree of model initial condition uncertainty. Therefore the forecast model covariance essentially resets itself during the summer period, which represents the high degree of uncertainty with early wintertime SWE forecasts.

[21] Error statistics are calculated for the 1359 half-degree pixels having coincident ground truth observations for the winter months (November to April) during the period of 1979 to 1987 (Figure 8a). Here the eastern coastal regions and western mountainous areas show the largest observed uncertainty in model SWE, reaching above 100 mm, while most Prairie, Tundra, and Taiga regions have very small observed uncertainty with values below 30 mm. The model-predicted uncertainties match the observed uncertainty very well in the Prairie and Great Lakes regions, are slightly too large in Tundra regions, and are too large in Taiga regions (Figures 8b and 8c).

Table 1. Statistics of Bias and Root Mean Square Error (RMSE) Between In situ Data and Model Open-loop run, Assimilation Run-I, and Assimilation Run-II for Pixels Only Including Five or More Ground Stations and With an In situ SWE Value Greater Than Zero[a]

		Bias, mm			RMSE, mm		
Experiment	Samples	Open loop	Assim-I	Assim-II	Open loop	Assim-I	Assim-II
A1	436	−51.21	−45.61	−9.06	50.67	40.36	40.28
A2	1422	9.70	−23.29	2.04	70.39	87.62	61.46
A3	10962	30.46	NA	8.66	96.65	NA	76.77

[a]Experiments 1–3 represent the cases shown in Figure 9a (January to March 1979), Figure 9b (July 1986 to June 1987), and Figure 11 (July 1979 to June 1987), respectively.

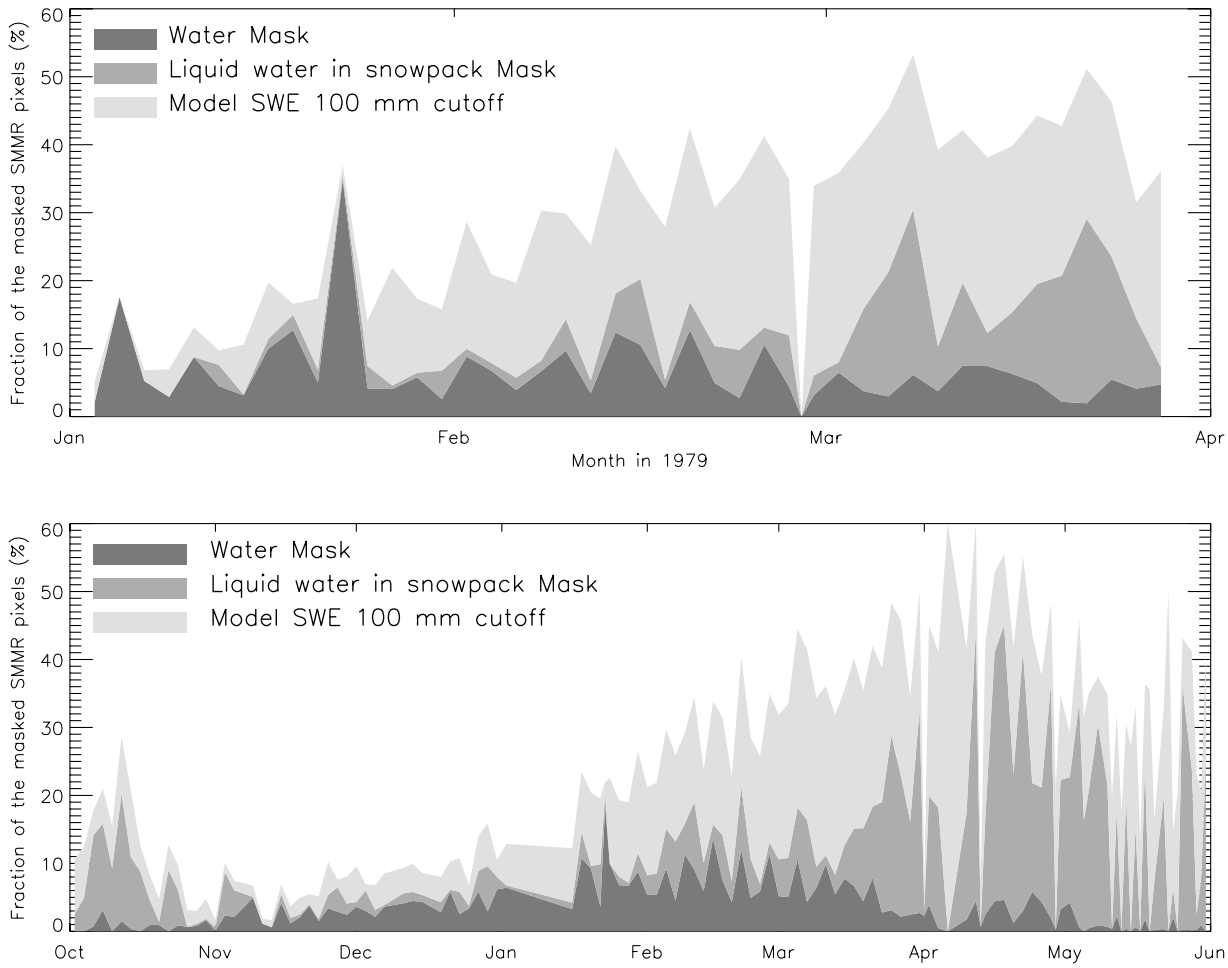

Figure 10. Fraction of SMMR SWE data omitted in response to each data quality rule for the periods (upper panel) January to March 1979 and (lower panel) October 1986 to May 1987.

However, there are no remotely sensed SWE estimates to be assimilated in the northern Canadian waterways with Tundra snow classification due to ice effects, meaning that the relatively poor uncertainty estimates in the Tundra region do not affect the model results. Likewise, there is typically no assimilation in the Taiga regions which are characterized with deep snowpacks (refer to Figure 2), with satellite observations typically eliminated due to the SWE being greater than 100 mm. In the western mountainous areas, the model-predicted uncertainty is largely underestimated, but the model-predicted uncertainty (above 40 mm) is approximately twice the estimated satellite observation uncertainty (less than 20 mm). Therefore the assimilation scheme will still put more reliance on the satellite SWE estimates than the model forecasts in this region.

4. Numerical Experiments

[22] A set of numerical experiments have been undertaken to evaluate the impact of assimilating quality-controlled SMMR SWE retrievals on snowpack state variables (snow water equivalent, snow depth, and heat content), using *Sun et al.'s* [2004] assimilation scheme, parameter specifications, and atmospheric forcing. Three model simulations (described below) were performed using the catchment-based land surface model for two periods: starting from (1) the middle of winter on 1 January 1 1979 and (2) from the middle of summer on 1 July 1 1986 (Figure 9). The initial conditions for these simulations were from a repeated 10-year simulation on a given year of forcing data, with the exception that all snowpack memory was erased at the initial time step. The snowpack state memory was erased so that erroneous model deep snowpack forecasts did not inadvertently prevent snowpack assimilation in the midwinter simulation.

[23] The first simulation is a straight model simulation run (referred to as the open-loop run) to show how the model performed in the absence of assimilation. The second and third simulations are two extended Kalman filter assimilation experiments (referred to as assimilation run-I and run-II), started with the same initial conditions as the open-loop run, but assimilating the remotely sensed SMMR SWE estimates when available. The difference between these two runs is that run-I assimilates all available SMMR SWE data while run-II only assimilates quality-controlled SMMR SWE data according to the three rules discussed earlier in this paper. A multiyear model open-loop run and remotely sensed SWE assimilation simulation (using assimilation run-II) are also presented for the entire SMMR duration from 1979 to 1987.

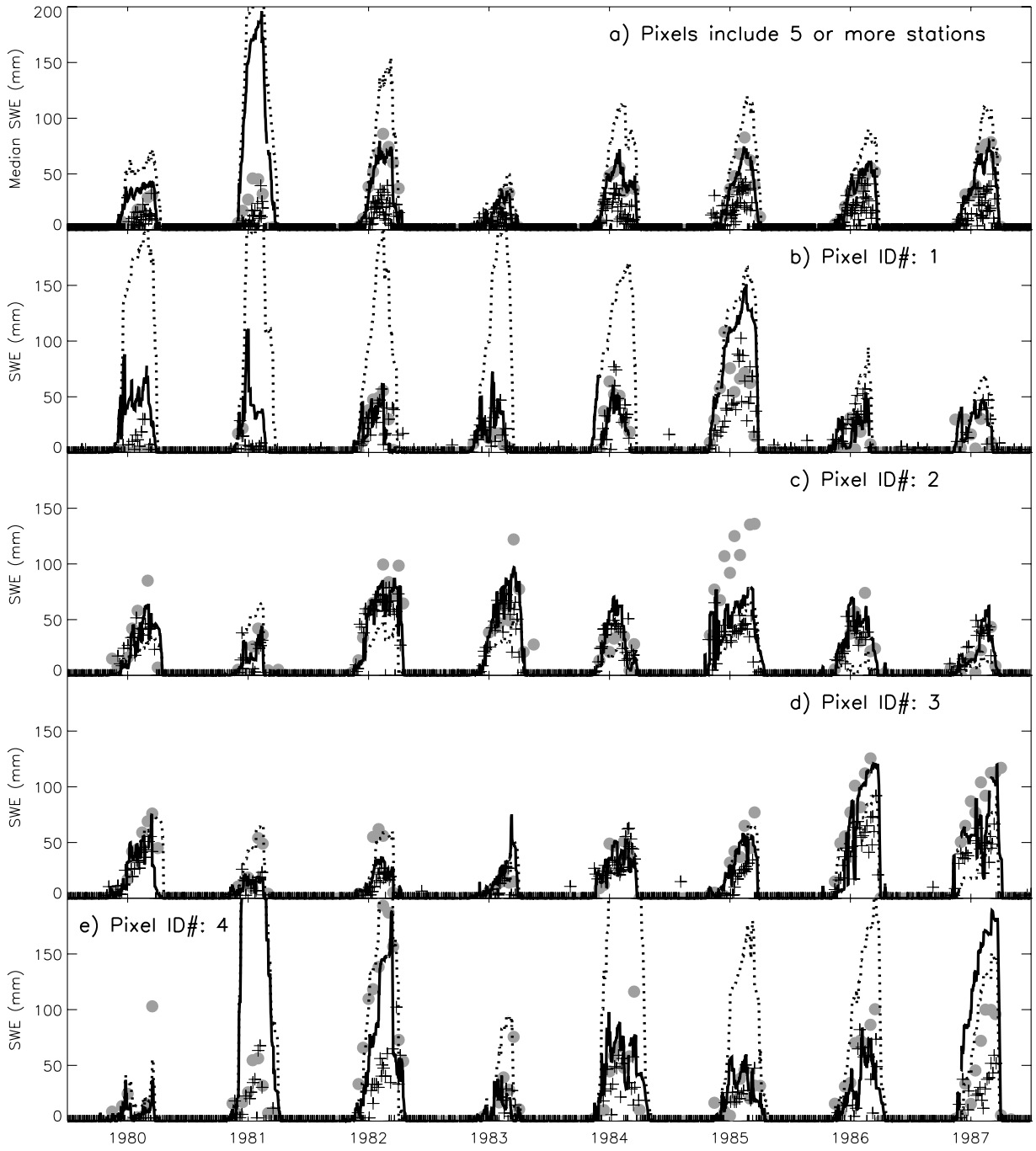

Figure 11. Comparison of the median SWE value for all pixels including five or more stations and the four representative pixels shown in Figure 1; ground observations (gray dots), SMMR observations (plus), model forecasts (dotted lines) and model forecast with assimilation (solid lines) from July 1979 to June 1987.

[24] To assimilate the regular grid SMMR SWE data into the catchment-based land surface model, the half-degree SMMR SWE data were first converted to the catchment domain. Therefore the assimilation was performed on a per catchment basis. When the open-loop simulation and assimilation were completed, the catchment-based output was then converted to half-degree pixels for comparison with half-degree averaged ground data. The results are evaluated using the Canadian in situ SWE measurements. Comparison of open-loop and assimilated model SWE estimates were made with the median in situ SWE value for pixels containing five or more in situ stations. The following statistical analysis has been performed using the median, as the arithmetic average value is often misleading if there are few outliers in the data.

5. Results and Discussion

[25] The median predicted and observed SWE estimates for pixels with five or more in situ stations are shown in

Table 2. Statistics of Bias and Root Mean Square Error (RMSE) Between In situ Data and Assimilation Output for Pixels Including Five or More Ground Stations and With an In situ SWE Value Greater Than Zero[a]

Experiment	Samples	Bias, mm	RMSE, mm
A3	10962	8.66	76.77
S1	10962	15.29	87.43
S2	10962	9.03	78.85

[a]Experiment A3 represents the case shown in Figure 11a (July 1979 to June 1987), Experiment S1 represents the sensitivity run by decreasing the model forecast error by a factor of 2 while increasing the observation error variance by a factor of 2, and Experiment S2 represents the sensitivity run by increasing the model forecast error by a factor of 2 while also decreasing the observation error variance by a factor of 2.

Figure 9. For the simulations starting in the middle of winter, it was found that assimilation run-II outperformed both of the other snowpack simulations, with the results from assimilation run-I approaching the unmasked SMMR SWE values. This was expected, as erroneous SWE observations when not eliminated (as in run-I) or adequately characterized by their error covariances act to degrade the snowpack simulation through their assimilation. The open-loop simulation significantly underestimates the snowpack SWE throughout the entire simulation due to the zero snow initialization. The resulting medians from assimilation run-II are in a close agreement with the ground observations. Statistical analysis shows that bias error has been largely reduced, and RMS error has been slightly reduced (Experiment A1 in Table 1).

[26] For the simulations starting in the middle of summer, the effects of initial SWE values were no longer important. However, once again, the simulated SWE from assimilation run-II showed the closest agreement with in situ SWE data, while the simulated SWE from assimilation run-I closely followed the unmasked SMMR SWE (also see Experiment A2 in Table 1). Moreover, in this case, the open-loop simulation overestimates the SWE.

[27] Given the success of the assimilation run-II algorithm, it is used in all subsequent analysis. Figure 10 shows the amount of SMMR data eliminated due to the application of the mask. The figure shows the individual impacts of the three mask criteria applied in the following order: (1) distance to open water, (2) liquid snow water presence in non coastal regions, and (3) snowpacks greater than 100-mm SWE. First, omission of SMMR SWE retrievals for regions within 200 km of significant open water bodies resulted in an approximately 5% reduction of available SMMR data, with varying fractions due to different snow-covered fractions and satellite tracks on a given day. Second, omission of SMMR SWE data due to liquid snow water presence resulted in an approximately 15% reduction of available SMMR data during autumn and spring months, with negligible reduction during midwinter. Finally, omission of the SMMR SWE for deep snowpacks resulted in an approximately 25% reduction of available SMMR data during midwinter to late winter. The combined effect is an approximately 20% elimination during early autumn, declining to an approximately 5% elimination for late autumn to mid winter, increasing linearly up to an approximately 50% elimination in spring. The few large spikes, such as Julian day 21 of the year 1979, result from the fact that most SMMR snow-covered areas within the satellite track at that day were located in the coastal areas. Conversely, the few large dips, such as Julian day 59 in 1979, result from the fact that few SMMR snow-covered areas are available within the satellite tracks at that day, and these few snow-covered areas are far from the coast with no liquid water presence or snowpacks greater than 100-mm SWE.

[28] A multiyear model simulation and assimilation run was performed for the entire SMMR duration from 1979 to 1987. Comparison of model simulation results was again made with median statistics for pixels including five or more in situ stations (Figure 11a). The model open-loop simulation overestimates the SWE by about 50 mm, while the unmasked satellite retrievals have an approximately 20 mm underestimation. Moreover, the assimilation simulation is in good agreement with the ground observations not only in the seasonal variations but also in the interannual variations (also see Experiment A3 in Table 1). The only exception is in 1981, with significant overestimation for both the open-loop and assimilation simulations. This is a result of significant atmospheric forcing errors in that year, with model-predicted SWE rapidly passing through the 100-mm cutoff, meaning that the simulation could not be constrained by assimilation of remotely sensed SWE estimates. This is also seen in Figure 11e.

[29] Two additional experiments, together with the above multiyear assimilation run (Experiment A3), were performed to test the sensitivity of the assimilation results to the uncertainty of the observation and models (Table 2). One experiment increased the observation error variance by a factor of 2 and decreased the model error variance by a factor of 2 (Experiment S1), with the other experiment reversing these changes to the error variances (Experiment S2). While Experiment S2 produced very similar results to Experiment A3, which reduced the bias from 30 mm in the open-loop run to about 9 mm and RMSE from 97 mm to 79 mm (77 mm for Experiment A3), Experiment S1 had a much larger bias (15 mm) and RMSE error (87 mm). This suggests that, in this case, the assimilation scheme is quite sensitive to increases in observation error and concurrent decreases in model error but insensitive to further reductions in observation error with a concurrent increase in model error due to the quality-controlled SMMR data used in all three experiments. Therefore the observation and model error covariance estimates used in Experiment A3 are appropriate for this study. These sensitivity experiments underscore the importance of obtaining accurate estimates of model and observation errors to achieve a good analysis. When the model error was erroneously underestimated in Experiment S1, the results were much worse than Experiments A3 and S2. Reducing model error in this study had a significant degrading effect on the analysis due to the poor model forecasts of SWE relative to the quality-controlled SMMR-derived SWE. This demonstrates the importance of validating analyses with independent data.

[30] To further evaluate the assimilation algorithm, comparisons are made for four individual pixels, each including five or more ground stations (Figures 11b–11e). The model simulation significantly overestimated the SWE at pixel number 1 (Alpine; 17 stations) and underestimated the SWE at pixel number 2 (Prairie; five stations) for most

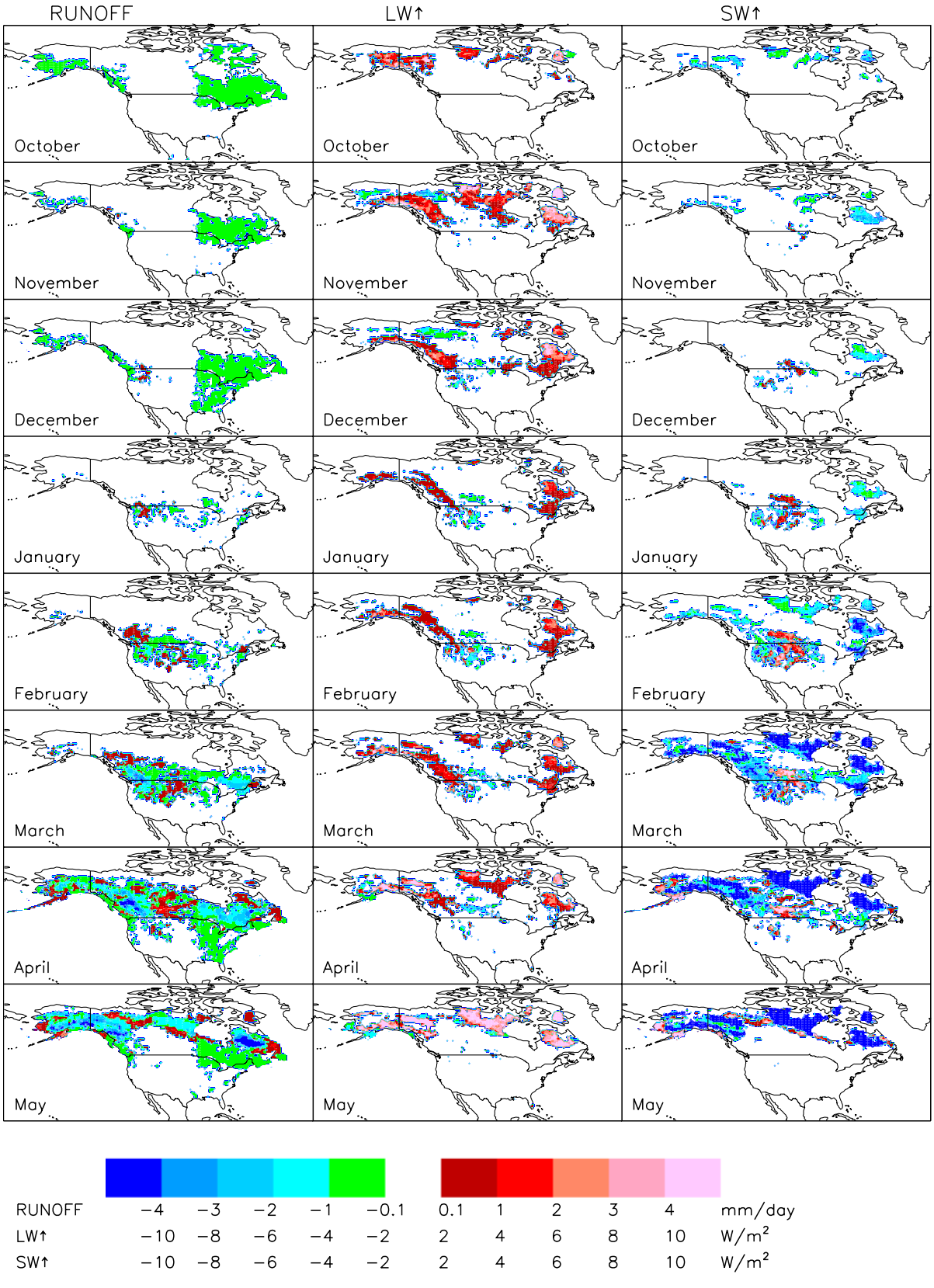

Figure 12. Difference between model forecast and model forecast with assimilation for monthly averaged total runoff (left column), upward longwave radiation (middle column), and upward shortwave radiation (right column) for winter months.

years, while unmasked SMMR estimates were in close agreements to the ground observations for both pixels. The assimilated SWE tends to approach both the SMMR and ground observations, as a result of the high-quality SMMR observations used in the assimilation at those locations. At pixel number 3 (Alpine; 11 stations), both SMMR and model SWE estimates are underestimated in the middle of the snow season of years 1986 and 1987. However, the assimilated SWE is close to ground observations in both these years because the assimilation algorithm optimally assimilated the relatively accurate SMMR SWE observations into the model during the early part of the snow season when the model performed most poorly. At pixel number 4 (Maritime; 27 stations), the model typically overestimated the SWE. Apart from 1981 and 1987, the assimilation of SMMR observations resulted in SWE estimates that closely followed the ground observations. The reason for poor assimilation results in those 2 years is a sudden erroneous transition by the model above the 100-mm SWE cutoff used to eliminate SMMR observations (in 1980–1981, this is due to the use of poor forcing data, and in 1986–1987, it is due to the assimilation of poor-quality SWE data). Beyond that time, the assimilation algorithm is no longer able to correct the model simulated snow water equivalent.

[31] Accurate estimation of snow water equivalent has important implications on climate forecasting through both freshwater inputs to the ocean from springtime snowmelt and upwelling radiation in response to surface albedo. Figure 12 shows the difference between the open-loop and assimilation simulations of monthly averaged total runoff and upward long and shortwave radiation. This comparison is for the winter months of October to May averaged over the years 1979–1987. While it is not possible to say which is better, there is a significant difference between the assimilation and open-loop forecasts, particularly during early spring. Assimilation runs modify the model simulation by significantly reducing runoff in the western mountainous area of Canada and the eastern Canada in spring and slightly reducing runoff in most regions of the eastern continent during the early snow season (October to December). Assimilation increases the upward longwave radiation for the whole snow season with significant increases in May and significantly reduces the upward shortwave radiation from February. Such large energy and water cycle differences could lead to significant climate model prediction differences. However, such changes in water and energy balance terms have not been verified as improvements using field measurements. Such substantiation is beyond the scope of this paper.

6. Conclusions

[32] Spatially complete and temporally continuous uncertainty maps for both remotely sensed and land surface model SWE estimates have been generated and evaluated. The remotely sensed SWE retrieval uncertainty is prescribed by a spatially constant monthly varying value, with data omitted under three considerations: (1) locations closer than 200 km to significant open water, (2) presence of liquid water in the snowpack, and (3) model SWE estimates greater than 100 mm. Model SWE uncertainty has been calibrated by tuning a spatially and temporally constant model error term used in the error propagation equations to the observed model error.

[33] A series of numerical experiments have demonstrated that assimilation of remotely sensed SWE estimates results in improved SWE estimates when compared to in situ measurements. However, when poor-quality observations are assimilated or the model simulation transitions are quickly beyond the 100-mm SWE cutoff, the assimilation algorithm is no longer able to improve the snowpack simulation. Comparison between the open-loop and assimilation simulations shows that runoff and upward short and long wave radiation are also modified through assimilation of remotely sensed SWE.

[34] **Acknowledgments.** The authors wish to thank three anonymous reviewers for their valuable comments. This work was funded by the National Aeronautics and Space Administration Earth Observing System Interdisciplinary Science (NASA EOS/IDS) Program NRA-99-OES-04.

References

Andreadis, K. M., and D. P. Lettenmaier (2006), Assimilating remotely sensed snow observations into a macroscale hydrology model, *Adv. Water Resour.*, *29*(6), 872–886.

Barnett, T. P., L. Dumenil, U. Schlese, E. Roechner, and M. Latif (1989), The effect of Eurasian snow cover on regional and global climate variations, *J. Atmos. Sci.*, *46*, 661–685.

Berg, A. A., J. S. Famiglietti, J. P. Walker, and P. R. Houser (2003), Impact of bias correction to reanalysis products on simulations of North American soil moisture and hydrological fluxes, *J. Geophys. Res.*, *108*(D16), 4490, doi:10.1029/2002JD003334.

Brown, R. D. (1996), Evaluation of methods for climatological reconstruction of snow depth and snow cover duration at Canadian meteorological stations, *Proc. Eastern Snow Conf.*, *53d Annual Meeting*, pp. 55–65, Williamsburg, VA.

Brown, R. D. (2000), Northern hemisphere snow cover variability and change, 1915–97, *J. Clim.*, *13*, 2335–2339.

Brown, R. D., and R. O. Braaten (1998), Spatial and temporal variability of Canadian monthly snow depths, 1946–1995, *Atmos. Ocean*, *36*(1), 37–54.

Chang, A. T. C., J. L. Foster, and D. K. Hall (1987), Nimbus-7 derived global snow cover parameters, *Ann. Glaciol.*, *9*, 39–44.

Chang, A. T. C., R. E. Kelly, E. G. Josberger, R. L. Armstrong, J. L. Foster, and N. M. Mognard (2005), Analysis of ground-measured and passive-microwave-derived snow depth variations in midwinter across the northern Great Plains, *J. Hydrometeorol.*, *6*(1), 20–33.

Clark, M. P., et al. (2006), Assimilation of snow covered area information into hydrologic and land-surface models, *Adv. Water Resour.*, in press.

Cohen, J., and D. Entekhabi (1999), Eurasian snow cover variability and Northern Hemisphere climate predictability, *Geophys. Res. Lett.*, *26*, 345–348.

Dong, J., J. P. Walker, and P. R. Houser (2005), Factors affecting remotely sensed snow water equivalent uncertainty, *Remote Sens. Environ.*, *97*, 68–82.

Foster, J. L., C. Sun, J. P. Walker, R. E. J. Kelly, A. T. C. Chang, J. Dong, and H. Powell (2005), Quantify the uncertainty in passive microwave snow water equivalent observations, *Remote Sens. Environ.*, *94*(2), 187–203.

Gelb, A. (1974), Optimal linear filtering, in *Applied Optimal Estimation*, edited by A. Gelb, pp. 102–155, MIT Press, Cambridge, Mass.

Houser, P. R., W. J. Shuttleworth, H. V. Gupta, J. S. Famiglietti, K. H. Syed, and D. C. Goodrich (1998), Integration of soil moisture remote sensing and hydrologic modeling using data assimilation, *Water Resour. Res.*, *34*(12), 3405–3420.

Koster, R. D., M. J. Suarez, A. Ducharne, M. Stieglitz, and P. Kumar (2000), A catchment-based approach to modeling land surface processes in a general circulation model: 1. Model structure, *J. Geophys. Res.*, *105*(D20), 24,809–24,822.

Liston, G. E., R. A. Pielke Sr., and E. M. Greene (1999), Improving first-order snow-related deficiencies in a regional climate model, *J. Geophys. Res.*, *104*, 19,559–19,567.

Loveland, T. R., B. C. Reed, J. F. Brown, D. O. Ohler, J. Zhu, L. Yang, and J. W. Merchant (2000), Development of a global land cover characteristics data set, *Int. J. Remote Sens.*, *21*, 1303–1330.

Lynch-Stieglitz, M. (1994), The development and validation of a simple snow model for the GISS GCM, *J. Clim.*, *7*, 1842–1855.

Mote, T. L., A. J. Grundstein, D. J. Leathers, and D. A. Robinson (2003), A comparison of modeled, remotely sensed, and measured snow water equivalent in the northern Great Plains, *Water Resour. Res.*, *39*(8), 1209, doi:10.1029/2002WR001782.

Namias, J. (1985), Some empirical evidence for the influence of snow on temperature and precipitation, *Mon. Weather Rev.*, *113*, 1542–1553.

Robinson, D. A., K. F. Dewey, and R. R. Heim (1993), Global snow cover monitoring: An update, *Bull. Am. Meteorol. Soc.*, *74*, 1689–1696.

Rodell, M., and P. R. Houser (2004), Updating a land surface model with MODIS-derived snow cover, *J. Hydrometeorol.*, *5*, 1064–1075.

Rodell, M., et al. (2004), The global land data assimilation system, *Bull. Am. Meteorol. Soc.*, *85*(3), 381–394.

Slater, A. G., and M. P. Clark (2006), Snow data assimilation via an Ensemble Kalman filter, *J. Hydrometeorol.*, *7*, 478–493.

Slater, A. G., et al. (2001), The representation of snow in land surface schemes: Results from PILPS 2 (d), *J. Hydrometeorol.*, *2*(1), 7–25.

Sturm, M., J. Holmgren, and G. E. Liston (1995), A seasonal snow cover classification system for local to regional applications, *J. Clim.*, *8*, 1261–1283.

Sun, C., J. P. Walker, and P. R. Houser (2004), A methodology for snow data assimilation in land surface model, *J. Geophys. Res.*, *109*, D08108, doi:10.1029/2003JD003765.

Tait, A., and R. Armstrong (1996), Evaluation of SMMR satellite-derived snow depth using ground-based measurements, *Int. J. Remote Sens.*, *17*, 657–665.

Walker, J. P., and P. R. Houser (2001), A methodology for initializing soil moisture in a global climate model: Assimilation of near-surface soil moisture observations, *J. Geophys. Res.*, *106*(D11), 11,761–11,774.

Yang, Z.-L., R. E. Dickinson, A. N. Hahmann, G.-Y. Niu, M. Shaikh, X. Gao, R. C. Bales, S. Sorooshian, and J. M. Jin (1999), Simulation of snow mass and extent in global climate models, *Hydrol. Processes*, *13*(12–13), 2097–2113.

Yang, F., A. Kumar, W. Wang, H. H. Juang, and M. Kanamitsu (2001), Snow-albedo feedback and seasonal climate variability over North America, *J. Clim.*, *14*, 4245–4248.

Yeh, T. C., R. T. Wetherald, and S. Manabe (1983), A model study of the short-term climate and hydraulic effects of sudden-snow cover removal, *Mon. Weather Rev.*, *111*, 1013–1024.

J. Dong, Hydrological Sciences Branch, NASA Goddard Space Flight Center, Code 614.3, Greenbelt, MD 20771, USA. (jiarui@hsb.gsfc.nasa.gov)

P. R. Houser, Climate Dynamics Department, College of Science, George Mason University and Center for Research on Environment and Water, Calverton, MD 20705-3106, USA.

C. Sun, Goddard Earth Sciences and Technology Center, University of Maryland Baltimore Country, Baltimore, MD 21250, USA.

J. P. Walker, Department of Civil and Environmental Engineering, The University of Melbourne, Parkville, Victoria 3010, Australia.